JCTC Journal of Chemical Theory and Computation

Article

pubs.acs.org/JCTC

Adsorption of Organic Molecules to van der Waals Materials: Comparison of Fluorographene and Fluorographite with Graphene and Graphite

František Karlický,[†] Eva Otyepková,[†] Rabindranath Lo,[‡] Michal Pitoňák,[§,∥] Petr Jurečka,[†] Martin Pykal,[†] Pavel Hobza,[†,‡] and Michal Otyepka*[,†]

[†]Regional Centre of Advanced Technologies and Materials, Department of Physical Chemistry, Faculty of Science, Palacký University Olomouc, tř. 17. listopadu 12, 77 146 Olomouc, Czech Republic

[‡]Institute of Organic Chemistry and Biochemistry, Academy of Sciences of the Czech Republic, v.v.i., Flemingovo nám. 2, 166 10 Prague 6, Czech Republic

[§]Department of Physical and Theoretical Chemistry, Faculty of Natural Sciences, Comenius University, Mlynská Dolina, 842 15 Bratislava, Slovakia

[∥]Computing Center of the Slovak Academy of Sciences, Dúbravská cesta č. 9, 845 35 Bratislava, Slovakia

Supporting Information

ABSTRACT: Understanding strength and nature of noncovalent binding to surfaces imposes significant challenge both for computations and experiments. We explored the adsorption of five small nonpolar organic molecules (acetone, acetonitrile, dichloromethane, ethanol, ethyl acetate) to fluorographene and fluorographite using inverse gas chromatography and theoretical calculations, providing new insights into the strength and nature of adsorption of small organic molecules on these surfaces. The measured adsorption enthalpies on fluorographite range from −7 to −13 kcal/mol and are by 1−2 kcal/mol lower than those measured on graphene/graphite, which indicates higher affinity of organic adsorbates to fluorographene than to graphene. The dispersion-corrected functionals performed well, and the nonlocal vdW DFT functionals (particularly optB86b-vdW) achieved the best agreement with the experimental data. Computations show that the adsorption enthalpies are controlled by the interaction energy, which is dominated by London dispersion forces (~70%). The calculations also show that bonding to structural features, like edges and steps, as well as defects does not significantly increase the adsorption enthalpies, which explains a low sensitivity of measured adsorption enthalpies to coverage. The adopted Langmuir model for fitting experimental data enabled determination of adsorption entropies. The adsorption on the fluorographene/fluorographite surface resulted in an entropy loss equal to approximately 40% of the gas phase entropy.

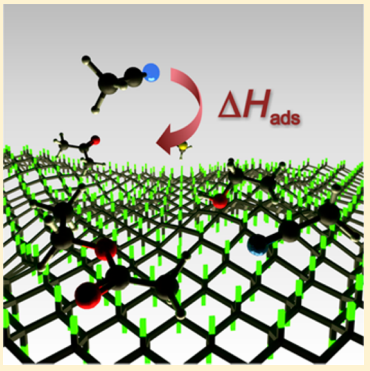

1. INTRODUCTION

Recently discovered two-dimensional (2D) materials such as graphene, fluorographene, graphene oxide, transition metal dichalcogenides, hexagonal boron nitride, and phosphorene all have very high surface/mass ratios, and many of their potential practical applications rely on their large surface areas. Consequently, there is a need to better understand their surface properties and the way in which their surfaces interact with their surroundings. In particular, there is great interest in the adsorption of molecules on 2D materials because of its technological importance. Small molecule adsorption can be used to tune the electrical properties of 2D materials[1] and is important in processes that can be exploited in mass,[2] gas,[3] and electrochemical[4] sensing. All kinds of sensors require a contact between an analyte and an active material to generate a readout, so it is essential to have a good understanding of the strength and nature of the interactions between adsorbed molecules and the sensing surface.[5] Fluorographene[6−8] (i.e., a fluorographite monolayer), fluorinated graphenes, and fluorographite are all active in electrochemical sensing and have sensing properties that depend on their C/F ratio and topology.[9] As such, they could potentially be used to create selective sensors in which specificity is achieved through the interaction of the analyte with an active zone consisting of a suitable fluorinated graphene. In addition to sensing applications, these materials can be used in gas separation and storage.[10,11] It has been demonstrated that adsorption to graphene is primarily controlled by London dispersive forces,[12] but little is known about adsorption to fluorographene and fluorographite. The few theoretical studies that have explored the adsorption of small molecules to fluorographene have suggested that it may have useful applications in hydrogen storage.[10,11,13,14]

Received: November 21, 2016
Published: February 1, 2017

DOI: 10.1021/acs.jctc.6b01130
J. Chem. Theory Comput. 2017, 13, 1328−1340

Table 1. Saturated Adsorption Enthalpies ΔH (in kcal/mol) and Entropies ΔS (in cal/molK) of Molecules on Fluorographite and Their Respective Confidence Intervals (for a 5% Level of Significance) Obtained by Inverse Gas Chromatography

compound	ΔH	ΔS	T_{min}-T_{max} [c]	ΔH_{cond} [d]	$\Delta H_{gr.}$ [e]
acetone[a]	−9.9 ± 0.5	−28 ± 1	303−333	−(7.3−7.0)	−8.2 ± 0.3[19]
acetonitrile[a]	−9.1 ± 0.4	−26 ± 1	303−328	−(8.3−8.1)	−7.6 ± 0.3[12]
dichloromethane[b]	−6.9 ± 1.3	−19 ± 4	303−323	−(7.3−6.9)	−5.9 ± 0.5[12]
ethanol[a]	−12.8 ± 1.0	−36 ± 3	303−353	−(10.1−9.2)	−12.0 ± 0.4[18]
ethyl acetate[b]	−12.4 ± 0.5	−32 ± 1	303−363	−(8.4−7.4)	−11.5 ± 0.2[12]

[a]Averaged over coverage values greater than 10%. [b]Averaged over coverage values over 2−20%. [c]The temperature interval T_{min}-T_{max} (in K) was used for data fitting (see the Supporting Information). [d]Standard enthalpies of condensation ΔH_{cond} (negative standard enthalpies of vaporization in kcal/mol) for T_{min} and T_{max} were adopted from the literature.[71] [e]Adsorption enthalpies (in kcal/mol) of the same molecules on graphene $\Delta H_{gr.}$ were taken from previous works.[12,18,19]

Adsorption enthalpies on surfaces are usually studied using adsorption calorimetry, temperature-programmed desorption, or equilibrium adsorption isotherms.[15] Recently, we witnessed a renaissance of inverse-gas chromatography (iGC) to study the process of adsorption. This technique measures retention characteristics of gas probes injected to a column loaded by analyzed material.[16,17] Its main advantage is that it provides results that represent averages over the sample's surface. In addition, adsorption enthalpies and entropies, and the dependence of these thermodynamic quantities on the surface coverage, can be obtained directly from iGC data.[12,18,19] It was shown that iGC provides adsorption enthalpies consistent with other experimental techniques.[20]

Quantum chemistry and solid-state physics calculations can be used to characterize intermolecular interactions and predict their strengths. However, deciphering the nature and strength of molecule−surface binding by computational means is frequently rather challenging because the binding energies are usually low and involve physical phenomena such as London dispersion forces that are difficult to model reliably;[21] physisorption forces are significantly weaker than chemisorption ones.[22,23] In finite molecular systems, the electron−electron correlation effects responsible for these noncovalent interactions can be described using the coupled cluster method, with single and double electron excitations being modeled iteratively and triple excitations perturbatively (CCSD(T)), or using the perturbative Møller−Plesset MP2.5 method (in which energies are calculated as the arithmetic mean of the MP2 and MP3 energies).[24] Unfortunately, these methods are not available for periodic systems, which are frequently superior to finite models when studying the adsorption of molecules on surfaces.[22] Consequently, methods based on density functional theory (DFT) are widely used in such applications. Classical general gradient approximation DFT methods are of semilocal character and thus cannot describe the long-range component of the London forces, which result from nonlocal electron−electron correlation. A range of theoretical methods has been developed to address this deficiency.[25] The performance of individual DFT methods is usually benchmarked against CCSD(T) or MP2.5 calculations on finite systems (molecular clusters), in order to identify approaches that accurately describe the system of interest. Both CCSD(T) as well as MP2.5 methods provide highly accurate interaction energies for various types of molecular clusters with errors of less than 2 and 4 relative percent, respectively.[24] CCSD(T) can be applied to complexes having up to around 35 heavy atoms, while MP2.5 can handle systems up to twice the size. Unfortunately, however, no reference method of comparable quality is currently available for use with periodic models, with the exception of the stochastic quantum Monte Carlo method,[22,26,27] that embody exceeding computational demands.

In this work, we determined isosteric adsorption enthalpies (ΔH) and isosteric adsorption entropies (ΔS) for five organic molecules (acetone, acetonitrile, dichloromethane, ethanol, and ethyl acetate) on fluorographite by iGC. We also performed extensive calculations on finite models of fluorographene to benchmark various DFT methods against CCSD(T) and MP2.5. The application of symmetry-adapted perturbation theory (SAPT)[28] to finite model systems allowed us to decipher the nature of the molecular interactions occurring on the fluorographene/fluorographite surfaces. Moreover, DFT calculations on periodic models helped us to clarify the roles of various adsorption sites and surface defects on adsorption to fluorographene, as well as the influence of molecular clustering. We conclude that the enthalpies of adsorption to fluorographene/fluorographite are slightly lower than those for graphene/graphite, i.e., small molecules generally bind more strongly to fluorographene and fluorographite than to their nonfluorinated counterparts.

2. RESULTS AND DISCUSSION

2.1. Isosteric Adsorption Enthalpies. Using iGC we determined the isosteric adsorption enthalpies of five molecular probes (Table 1) to fluorographite for coverage values ranging from 2 to 20% of the adsorbate monolayer. The isosteric adsorption enthalpies of acetone, acetonitrile, and ethanol decreased as the surface coverage increased, with saturation occurring at a coverage level slightly above 10% (Figure 1). The isosteric adsorption enthalpies of ethyl acetate and dichloromethane were rather coverage-independent. The saturated adsorption enthalpies $\Delta H \pm \delta\Delta H$ reported in Table 1 ranged from −6.9 kcal/mol (dichloromethane) to −12.8 kcal/mol (ethanol). The measured enthalpies suggest that the studied molecules adsorb by physisorption.

When explaining coverage dependence of the adsorption enthalpies, one should take into account the fact that the real material surface is really complex containing various structural and chemical features and defects, e.g., edges, steps, cavities, pores, vacancies, or adatoms. Such features may represent sites, where the adsorbate preferentially binds (the high-energy sites[19]). In addition, some adsorbates may tend to form clusters over the surface.[18] As the iGC provides averaged adsorption enthalpies over the surface all these effects are involved. Fortunately, the complexity of the process can be typically deciphered from the plot of adsorption enthalpy vs coverage in combination with atomistic simulations. The decreasing adsorption enthalpies of acetone, acetonitrile, and ethanol with increasing coverage (Figure 1) can be explained by the

DOI: 10.1021/acs.jctc.6b01130
J. Chem. Theory Comput. 2017, 13, 1328−1340

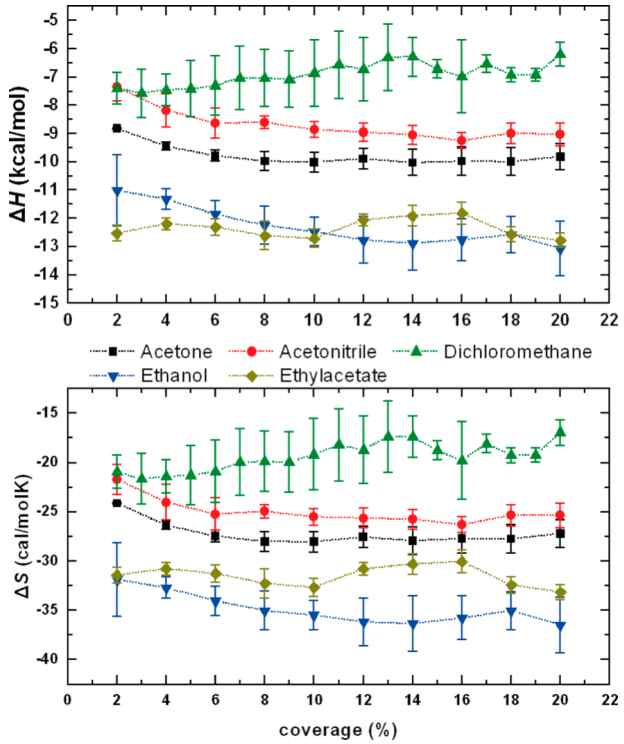

Figure 1. Isosteric adsorption enthalpies ΔH (top) and entropies ΔS (bottom) for five organic molecules on fluorographite obtained from inverse gas chromatography as a function of surface coverage. The dotted lines are eye-guides.

clustering of these molecules over the adsorbent surface, because the same behavior was observed for ethanol adsorption to graphene and was attributed to ethanol clustering over the graphene surface.[18] This behavior might occur when the adsorption enthalpy of a single molecule to the surface is greater than the enthalpy of condensation; however, we should note that a tendency of clustering is given by a delicate balance among adsorption enthalpy, enthalpy, and entropy of clustering.[18] The rather constant adsorption enthalpies of dichloromethane to the surface (at very low coverage levels; see Figure S1 in the Supporting Information) may indicate that the material used in this work had few high-energy sites or that the enthalpies of adsorption to structural features that typically correspond to high energy sites (e.g., steps, edges, cavities, and defects) are comparable to those for adsorption to a fluorographene/fluorographite surface lacking such features. Computational methods (see below) were used to determine which of these potential explanations was most plausible.

We measured the adsorption enthalpies of the same probe molecules to graphene powder in a previous investigation.[12,18,19] On comparing the adsorption enthalpies for fluorographene/fluorographite and graphene/graphite, we found that the enthalpies of adsorption to fluorographite are generally slightly lower than those for graphene/graphite (by 1.2 kcal/mol on average, corresponding to 14% of the ΔH for graphene; see Table 1). This indicates that small organic molecules bind more strongly to fluorographite than to graphite and hence that fluorographene/fluorographite more readily adsorbs guest molecules from its environment.

2.2. Benchmarking of Theoretical Methods. We used finite systems to benchmark the accuracy of selected DFT methods when applied to the systems of interest and used the best-performing methods in these benchmarking studies to perform further calculations on periodic-boundary models. Two small models of fluorographene/fluorographite surfaces were used in the benchmarking calculations. The smallest model, perfluorohexamethylcyclohexane ($C_{12}F_{24}$), was small enough to permit the use of the CCSD(T) method, which provides very accurate interaction energies ΔE_i for a wide range of complexes. However, because of the small size of this model, it may not constitute an adequate representation of the theoretically infinite fluorographene/fluorographite surface. We therefore also considered a larger model, hexatriacontafluorotetracosahydrocoronene ($C_{24}F_{36}$), which is more representative and was also used to obtain geometries and enthalpy corrections (see Methods). Because it was computationally unfeasible to perform CCSD(T) calculations on this larger system, we instead performed reference calculations using the MP2.5 method, which is known to approach the quality of CCSD(T) for many noncovalent complexes.[29] The use of MP2.5 in this case was validated by comparing the energies calculated with this method for the smaller $C_{12}F_{24}$ system to those obtained with CCSD(T). Both CCSD(T) and MP2.5 explicitly model the dispersion energy, whereas most DFT methods model it implicitly using some kind of correction.[30] This is one of the reasons why the performance of dispersion-corrected DFT techniques must be carefully tested.

The CCSD(T) and MP2.5 interaction energies for the dichloromethane and ethanol complexes of $C_{12}F_{24}$ were in reasonably good agreement (Table 2), although the CCSD(T) interaction energies are systematically more attractive (by 10% on average) than the MP2.5 energies. This justified the use of the less expensive MP2.5 method as a source of reference data for calculations on the large models. DFT functionals with London dispersion corrections generally provided reasonably accurate energies for the smaller complexes (Table 2, Figure 2, Figure S2), but optB86b-vdW and vdW-DF overestimated the interaction energy by over 30% for this model. However, it should be noted that the optB88-vdW functional provided the best agreement with experimental data in a study on the adsorption of small molecules to graphene.[12] This may indicate that the individual dispersion-corrected DFT methods do not provide a consistent treatment of dispersion interactions for finite size and periodic systems. Together with the limited amount of available experimental data on such systems, this complicates the assessment of theoretical methods for adsorption studies.

Table 3 summarizes the interaction energies calculated for complexes of the larger $C_{24}F_{36}$ system with the five organic molecules using MP2.5 and various DFT functionals. The

Table 2. Interaction Energies ΔE_i (in kcal/mol) of Five Organic Molecules with Perfluorohexamethylcyclohexane ($C_{12}F_{24}$)

compound	CCSD(T)	MP2.5	PBE-D2	PBE-D3	PBE-TS	PBE-TS+SCS	optB86b-vdW	vdW-DF	vdW-DF2
dichloromethane	−2.7,[a] −2.9[b]	−2.4,[a] −2.6[b]	−3.0	−2.6	−2.7	−2.5	−3.8	−3.8	−2.9
ethanol	−3.1,[a] −3.3[b]	−2.7,[a] −2.8[b]	−3.8	−3.3	−3.5	−3.3	−4.3	−4.2	−3.4

[a]Using MP2-F12/cc-pVDZ-F12 ΔE. [b]Using MP2/CBS ΔE.

DOI: 10.1021/acs.jctc.6b01130
J. Chem. Theory Comput. 2017, 13, 1328−1340

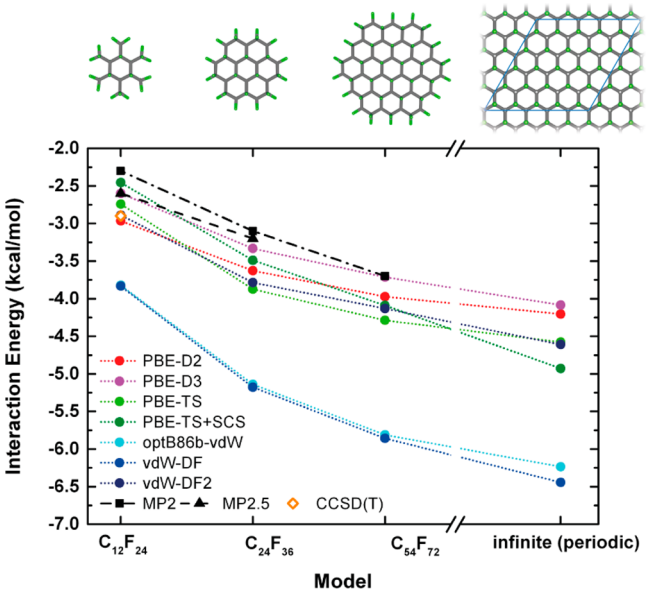

Figure 2. Models of fluorographene (top) and their interaction energies ΔE_i with dichloromethane, showing the dependence of the interaction energy on the size of the model system and the computational method used (bottom). Dark gray and green represent C and F atoms, respectively.

MP2.5 results suggest that the complexes with the largest and smallest interaction energies are those of ethyl acetate and dichloromethane, respectively, and all of the tested functionals replicated this trend. The optB86b-vdW and vdW-DF functionals again strongly overestimated the absolute interaction energies (by more than 56%), whereas the B97-D3 functional underestimated the interaction energies by more than 25%. Other DFT functionals provided interaction energies that agreed reasonably well with the reference MP2.5 values. The B3LYP-D3 and PBE-D3 functionals gave the most accurate interaction energies with respect to MP2.5 (with deviations below 10%); however, PBE-D2, PBE-TS+SCS, and vdW-DF2 functionals performed also well because the CCSD(T) energies were more negative than the MP2.5 values for the smaller model.

2.3. Model Size. To determine how the interaction energy ΔE_i depends on the model size, we performed calculations on a larger finite model system - $C_{54}F_{72}$. We also compared all of the results obtained using finite size models to results for an infinite (periodic) model based on a 5 × 5 fluorographene supercell. This comparison was justified by the fact that the calculated adsorption configurations on fluorographene were similar to those for the finite models (Figure 3). Interaction energies for small molecules on all four models of fluorographene ($C_{12}F_{24}$, $C_{24}F_{36}$, $C_{54}F_{72}$, and periodic $C_{50}F_{50}$; see Figure 2) could be computed using DFT methods implemented in the VASP package (see the Methods section), namely the empirically corrected density functionals PBE-D2, PBE-D3, PBE-TS, and PBE-TS-SCS, as well as the nonlocal correlation functionals vdW-DF, vdW-DF2, and optB86b-vdW. We also performed less expensive wave function-based calculations using the MP2/aug-cc-pVDZ method to compare the interaction energies computed in this way for the three finite systems ($C_{12}F_{24}$, $C_{24}F_{36}$, and $C_{54}F_{72}$) to those obtained by DFT.

Figures 2 and S2 present the results of the calculations performed for the adsorption of dichloromethane (and ethanol) on all four fluorographene model systems using various methods. In all cases, the calculated interaction energy decreased as the model size increased, i.e. the small molecules were most strongly bound on periodic fluorographene. The ratio of MP2.5/CBS interaction energies of dichloromethane and ethanol molecules with $C_{24}F_{36}$ and $C_{12}F_{24}$ equals to 1.2 and 1.3, respectively. The same ratio of MP2/aug-cc-pVDZ for dichloromethane complexes equals to 1.4, whereas it becomes 1.2 when we consider $C_{54}F_{72}$ and $C_{24}F_{36}$ models. It should be noted here that MP2.5 and MP2 describe the dispersion energy explicitly, which means that they model well both pairwise and many-body energy terms[31] (however, strictly speaking, MP2 does not provide reliable values for the many-body dispersion term[32]). This is not necessarily true for DFT methods.[33−35] The ratios of the calculated energies of the dichloromethane and ethanol complexes of $C_{24}F_{36}$ and $C_{12}F_{24}$ obtained with different DFT methods were generally similar to the MP2.5 values (in the cases of PBE-D2, PBE-D3, vdW-DF2, and optB86b-vdW) or the MP2 values (for PBE-TS, PBE-TS-SCS, and vdW-DF). Moreover, the DFT interaction energy ratios for the $C_{54}F_{72}$ and $C_{24}F_{36}$ models were similar to those obtained

Table 3. Interaction Energies ΔE_i (in kcal/mol) of Five Organic Molecules to Perfluorotetracosahydrocoronene ($C_{24}F_{36}$)[b]

compound	MP2.5/CBS	B97-D3/TZVPP	B3LYP-D3/TZVPP	M06-2X/cc-pVTZ	PBE-D3/TZVPP[a]	PBE-D3/PW[a]	PBE-D2/PW	PBE-TS/PW	PBE-TS+SCS/PW	optB86b-vdW/PW	vdW-DF/PW	vdW-DF2/PW
acetone	−4.6	−3.1	−4.6	−4.2	−4.7	−4.6	−5.0	−5.7	−5.1	−7.0	−7.2	−5.2
		(−33%)	(0%)	(−9%)	(2%)	(0%)	(8%)	(23%)	(11%)	(51%)	(56%)	(13%)
acetonitrile	−3.6	−2.5	−3.5	−3.1	−3.7	−3.7	−3.9	−4.5	−4.2	−5.3	−5.6	−4.1
		(−31%)	(−3%)	(−14%)	(3%)	(3%)	(8%)	(25%)	(16%)	(48%)	(56%)	(14%)
dichloromethane	−3.2	−2.5	−3.5	−2.5	−3.5	−3.3	−3.6	−3.9	−3.5	−5.1	−5.2	−3.8
		(−22%)	(9%)	(−22%)	(9%)	(4%)	(13%)	(21%)	(9%)	(61%)	(62%)	(18%)
ethanol	−3.5	−2.9	−4.3	−3.7	−4.3	−4.1	−4.5	−5.1	−4.7	−5.7	−5.7	−4.4
		(−17%)	(23%)	(6%)	(23%)	(16%)	(29%)	(45%)	(36%)	(63%)	(62%)	(25%)
ethyl acetate	−5.7	−3.9	−5.9	−5.2	−6.0	−6.0	−6.5	−7.3	−6.7	−9.2	−9.4	−6.9
		(−32%)	(4%)	(−9%)	(5%)	(5%)	(14%)	(28%)	(18%)	(61%)	(65%)	(20%)
average of percentage error		−27%	7%	−10%	8%	6%	15%	28%	18%	57%	60%	18%

[a]We obtained near-identical PBE-D3 interaction energies by two different approaches: using localized Gaussian orbitals (the TZVPP basis set) as implemented in Turbomole and using plane waves (PW) as implemented in VASP (see also the Methods section). [b]The relative deviation from the MP2.5 energy, $(\Delta E_i^{DFT}-\Delta E_i^{MP2.5})/\Delta E_i^{MP2.5}$, is given in parentheses.

DOI: 10.1021/acs.jctc.6b01130
J. Chem. Theory Comput. 2017, 13, 1328−1340

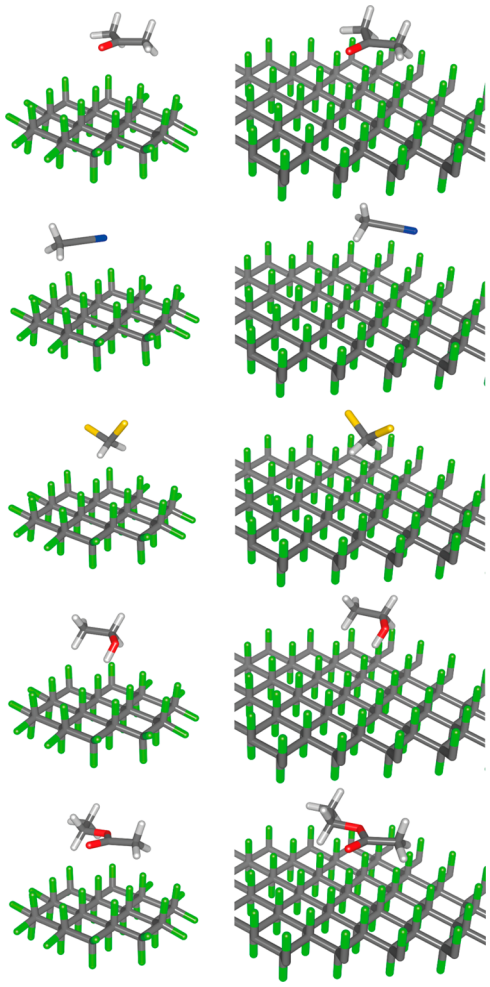

Figure 3. Adsorption geometries of acetone, acetonitrile, dichloromethane, ethanol, and ethyl acetate (from the top to the bottom, respectively) on perfluorinated tetracosahydrocoronene (left column) and fluorographene (right column). Structures shown in the left and right columns were obtained by optimization with the B97D and optB86b-vdW density functionals, respectively. Dark gray, green, red, blue, yellow, and white represent C, F, O, N, Cl, and H atoms, respectively.

with MP2. The tested DFT methods thus predict the effects of increasing surface size similarly to MP2.5 and MP2, both of which correctly model many-body terms.

The interaction energies calculated for the largest finite model system, $C_{54}F_{72}$, were only slightly (0.2−0.8 kcal/mol) higher than those for the infinite periodic surface (Figures 2 and S2). This suggests that calculations on $C_{54}F_{72}$ provide quite good estimates of interaction energies for fluorographene. In addition, the relative ordering of the interaction energies for the studied small molecules on $C_{54}F_{72}$ matched that for the periodic system.

The calculated interaction energies obtained for the periodic model system with different density functionals decreased in the following order: $\Delta E_i^{\text{PBE-D3}} > \Delta E_i^{\text{PBE-D2}} > \Delta E_i^{\text{vdW-DF2}} > \Delta E_i^{\text{PBE-TS}}$, $\Delta E_i^{\text{PBE-TS+SCS}} > \Delta E_i^{\text{vdW-DF}}$, $\Delta E_i^{\text{optB86b-vdW}}$ (see the interaction curves in Figure S3). The interaction energies provided by the DFT-D3 and optB86b-vdW/vdW-DF functionals thus corresponded to the upper and lower limits of the DFT energy range, which spanned approximately ∼3 kcal/mol on average (∼5 kcal/mol for ethyl acetate). The DFT energies calculated for the finite $C_{24}F_{36}$ model were less variable (spanning a range of ∼2 kcal/mol for all small molecules other than ethyl acetate; see Table 3), and those for the smallest $C_{12}F_{24}$ model varied still less, with a range of ∼1 kcal/mol (Table 2).

2.4. The Nature of the Bonding in the Adsorption Complexes. The calculations performed using the DFT functionals with empirical dispersion corrections indicated that dispersion interactions are the most important component of the interaction energy resulting from the binding of small molecules to the fluorographene surface. The pure PBE functional yielded a very shallow potential well for molecular adsorption to fluorographene (<1 kcal/mol, Figure S3), but substantially more negative adsorption energies were obtained using functionals with dispersion corrections. Based on the adsorption energies computed using the many-body D3 dispersion correction, dispersion accounted for 92% of the total binding energy ($\Delta E^{\text{D3}}/\Delta E^{\text{PBE-D3}}$) in the case of acetone, 64% for acetonitrile, 69% for dichloromethane, 73% for ethanol, and 83% for ethyl acetate. This trend was confirmed by more rigorous DFT based symmetry adapted perturbation theory (DFT-SAPT)[28] calculations on the intermediate finite model $C_{24}F_{36}$ (see Figure 4). The dispersion contribution

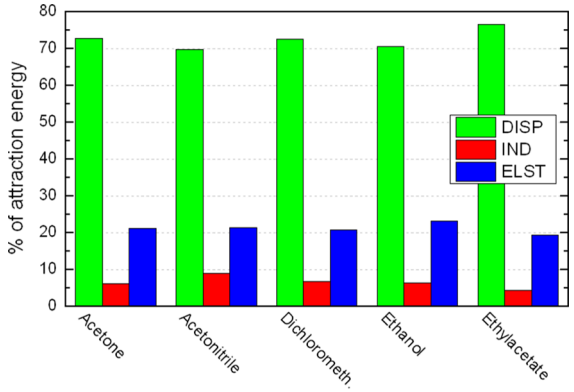

Figure 4. Decomposition of the total attractive energy into dispersion, induction, and electrostatic contributions calculated by DFT-SAPT for the small model system $C_{24}F_{36}$.

(calculated as $\Delta E_i^{\text{disp}}/(\Delta E_i^{\text{disp}} + \Delta E_i^{\text{ind}} + \Delta E_i^{\text{elst}})$ dominated, accounting for 72%, 70%, 73%, 70%, and 76% of the total attractive interaction energies for acetone, acetonitrile, dichloromethane, ethanol, and ethyl acetate, respectively. The electrostatic term (19−23%) represented the second largest attractive contribution, followed by the induction or polarization term (4−9%); see Figure 4. This trend is similar to that observed for the interaction of small molecules with a finite model of graphene (coronene, see Table S1 for a comparison). In the graphene case, the interactions were similarly dominated by dispersion (62−66%), with lesser contributions from electrostatics (26−29%) and induction (8−12%).[12] The relative contribution of electrostatics to binding in the case of $C_{24}F_{36}$ was lower than that for graphene, which is somewhat surprising given that C−F bonds are highly polar (to the extent that they have been labeled "semi-ionic"[36]), making the distribution of electron density across the fluorographene plane rather inhomogeneous.[37]

2.5. Contributions to the Adsorption Enthalpies. Data for the hexatriacontafluorotetracosahydrocoronene model system ($C_{24}F_{36}$; see Figure 3) were used to estimate the

DOI: 10.1021/acs.jctc.6b01130
J. Chem. Theory Comput. 2017, 13, 1328−1340

Table 4. Adsorption Energies (in kcal/mol) and Other Quantities[a] Characterizing the Adsorption of Five Organic Molecules on Perfluorinated Tetracosahydrocoronene

compound	ΔE	ΔE_0	ΔU	ΔH	ΔG	$\Delta\Delta E_0$	$\Delta\Delta E_T$	$\Delta\Delta E_H$	$\Delta\Delta E_G$	ΔH-ΔE	ΔS
acetone	−6.3	−5.4	−4.2	−4.8	5.1	0.9	1.2	−0.6	9.9	1.5	−31.7
acetonitrile	−4.4	−4.0	−2.6	−3.2	3.4	0.4	1.4	−0.6	6.6	1.2	−21.1
dichloromethane	−4.5	−4.3	−2.6	−3.3	3.4	0.2	1.7	−0.6	6.6	1.3	−21.2
ethanol	−6.3	−5.5	−4.2	−4.8	3.9	0.8	1.3	−0.6	8.6	1.5	−27.6
ethyl acetate	−8.6	−7.8	−6.5	−7.1	3.0	0.7	1.3	−0.6	10.1	1.5	−32.3

[a] ΔE and ΔE_0 with and without ZPE, respectively, internal energies ΔU, enthalpies ΔH, Gibbs energies ΔG, and entropies ΔS (in cal/molK), and the contributions of the zero-point energy ($\Delta\Delta E_0$), thermal ($\Delta\Delta E_T$), enthalpy ($\Delta\Delta E_H$), and Gibbs energy corrections ($\Delta\Delta E_G$). The adsorption process $C_{24}F_{36} + X \rightarrow C_{24}F_{36}\cdots X$ was modeled at 313.15 K and 101.325 kPa using the B97D functional.

Table 5. Adsorption Energies and Enthalpies of Five Organic Molecules on Periodic Fluorographene in kcal/mol Calculated with Various Density Functionals[a]

	PBE-D2		PBE-D3		PBE-TS		PBE-TS+SCS		optB86b-vdW		vdW-DF		vdW-DF2	
compound	ΔE	ΔH	ΔE	ΔH	ΔE	ΔH	ΔE	ΔH	ΔE	ΔH	ΔE	ΔH	ΔE	ΔH
acetone	−6.6	−5.1	−7.6	−6.1	−8.0	−6.5	−8.5	−7.0	−10.7	−9.3	−9.7	−8.3	−9.9	−8.4
acetonitrile	−6.6	−5.4	−6.1	−4.9	−6.2	−5.0	−6.6	−5.5	−7.8	−6.6	−7.0	−5.8	−7.6	−6.4
dichloromethane	−6.4	−5.1	−6.1	−4.8	−6.3	−5.1	−6.9	−5.6	−7.9	−6.7	−6.8	−5.5	−7.4	−6.2
ethanol	−7.6	−6.1	−6.8	−5.3	−7.0	−5.5	−7.5	−6.0	−8.7	−7.2	−7.5	−6.1	−8.4	−6.9
ethyl acetate	−10.4	−9.0	−9.5	−8.0	−10.4	−8.9	−11.4	−10.0	−13.8	−12.3	−12.8	−11.3	−12.2	−10.8

[a] The correction to the adsorption enthalpy was obtained from calculations on perfluorotetracosahydrocoronene (Table 4).

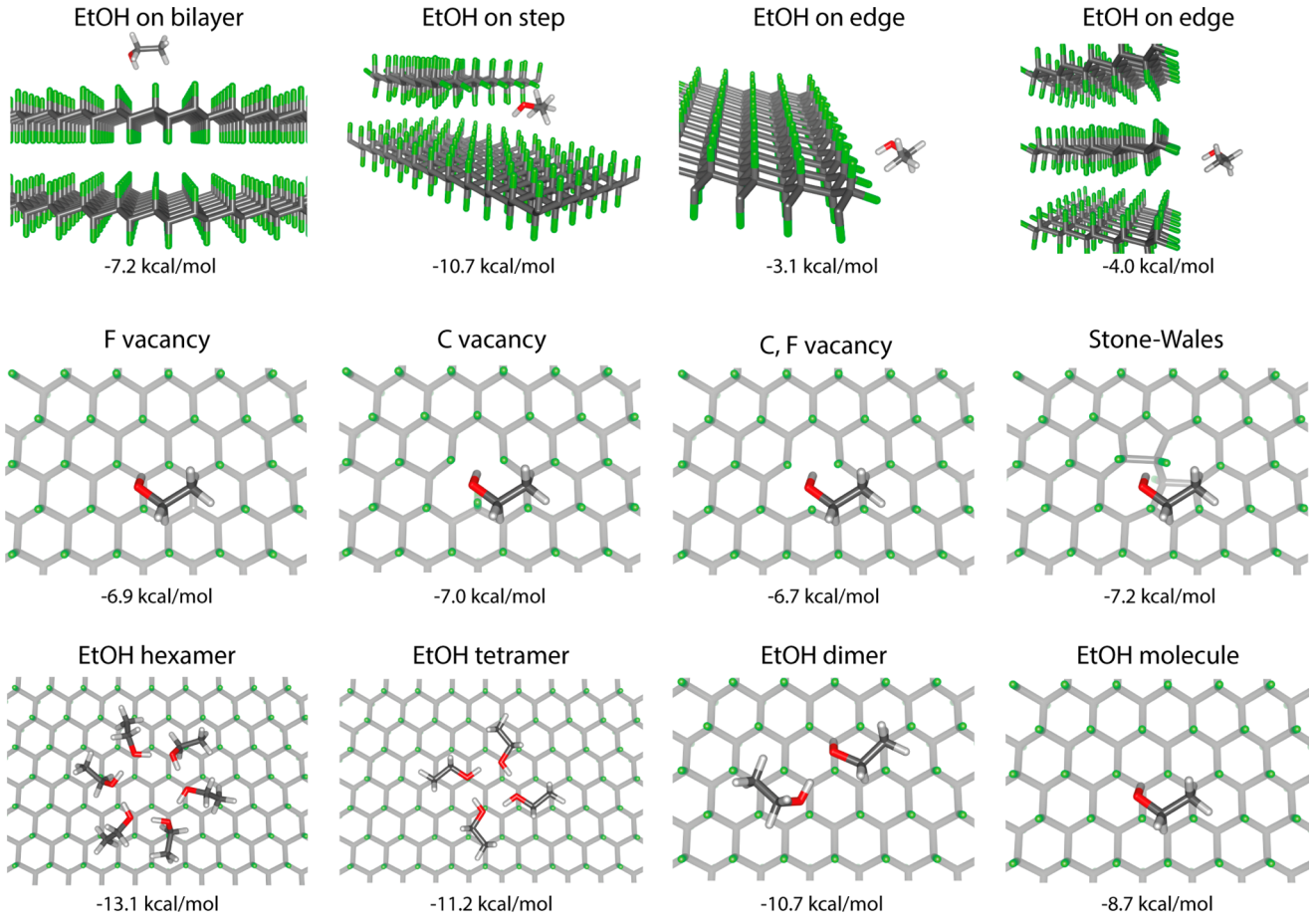

Figure 5. Adsorption geometries of an ethanol molecule on multilayer fluorographene and a fluorographene step/edge (top). Adsorption geometries of an ethanol molecule on fluorographene with vacancy defects and a Stone−Wales defect (middle). Clustering of ethanol molecules (bottom). All adsorption energies were obtained with the optB86b-vdW density functional. For molecular clusters, the quoted energies are normalized to one molecule.

DOI: 10.1021/acs.jctc.6b01130
J. Chem. Theory Comput. 2017, 13, 1328−1340

Table 6. Adsorption Energies (in kcal/mol) of Five Organic Molecules on Fluorographene Steps and Defect-Free Surfaces[a]

compound	ΔE^{step}	$\Delta E^{surface}$	difference
acetone	−13.3 (−8.1)	−10.7 (−7.6)	−2.6 (−0.5)
acetonitrile	−11.2 (−6.3)	−7.8 (−6.1)	−3.4 (−0.2)
dichloromethane	−11.6 (−7.1)	−7.9 (−6.1)	−3.7 (−1.0)
ethanol	−10.7 (−6.6)	−8.7 (−6.8)	−2.0 (0.2)
ethyl acetate	−16.8 (−10.2)	−13.8 (−9.5)	−3.1 (−0.7)

[a]Calculated with the optB86b-vdW density functional (results obtained with PBE-D3 in parentheses).

different contributions to the adsorption enthalpies of small molecules[12] on fluorographene (Table 4) by applying standard expressions from statistical mechanics under the ideal gas, rigid rotor, and harmonic oscillator approximations. The derived enthalpy/energy differences ($\Delta H - \Delta E$) ranged from 1.2 to 1.5 kcal/mol and were used as corrections to derive adsorption enthalpies from the adsorption energies calculated for the periodic model. These adsorption energies ranged from −7.8 to −13.8 kcal/mol (optB86b-vdW functional, Table 5) and dominated the calculated adsorption enthalpies because the correction terms were equal to at most ∼19% of the calculated interaction energies. The same trend was previously observed for adsorption to graphene.[12]

2.6. The Roles of High-Energy Sites, Surface Irregularities, and Defects. We investigated the potential contributions of surface irregularities, defects, and molecular configurations to the adsorption process by studying the roles of (i) multilayers, (ii) surface steps and edges, and (iii) surface defects (Figure 5). Specifically, we compared the adsorption of ethanol on monolayer and bilayer fluorographene, because studies on graphene had previously shown that adsorption to multilayer graphene was slightly stronger than that to a graphene monolayer.[18,19] Conversely, the energy of adsorption for small molecules on bilayered fluorographene was 1.4 kcal/mol higher than that for a fluorographene monolayer (Table S2, Supporting Information). The addition of a third layer of fluorographene changed the adsorption energy by less than 0.1 kcal/mol relative to that for the bilayer.

Steps are regarded as high-energy sites in multilayered graphene and graphite because the energy change upon adsorption to steps is up to 2.5 times greater than that for adsorption to a stepless surface. Such effects are easily detected in iGC experiments.[18,19] In the case of fluorographene, the calculated adsorption energies on steps were only 10−20% lower than those for the stepless surface (Table 6). Taking into account Boltzmann distribution of probes between the high-energy sites and surface,[19] such differences are barely experimentally detectable, as demonstrated by the corresponding iGC data (*cf.* section 2.1). In addition, the calculated adsorption energies for ethanol on fluorographene edge sites were *less* favorable (−4.0 and −3.1 kcal/mol) than those for the surface (−8.7 kcal/mol, Figure 5).

We also considered four types of defect sites: (i) F vacancies, (ii) C vacancies, (iii) C−F vacancies, and (iv) Stone−Wales (SW) defects, the latter corresponding to lattice reconstructions in which four hexagons were transformed into two pentagons and two heptagons [an SW(55−77) defect] (Figure 5). Ethanol bound preferentially to the defect-free surface: its adsorption energies on the defect sites (−6.7 to −7.2 kcal/mol) were less negative than those for the perfect surface (−8.7 kcal/mol).

2.7. Clustering on the Surface. The experiments indicated that clustering played a significant role in the adsorption of ethanol, acetonitrile, and acetone to fluorographene/fluorographite (*cf.* section 2.1 and Figure 1). To clarify its effects, we explored the binding of ethanol clusters to fluorographene. Our calculations revealed the formation of cyclical planar ethanol clusters lying flat on the fluorographene surface (Figure 5). The adsorption energies of ethanol dimers, tetramers, and hexamers on fluorographene were −10.7 kcal/mol, − 11.2 kcal/mol, and −13.1 kcal/mol per molecule, respectively, and were lower than the adsorption energy of single molecules (−8.7 kcal/mol). This strongly suggests that ethanol forms clusters on fluorographene surfaces and that the measured adsorption enthalpies corresponded to the binding of ethanol clusters. Similar analyses were then performed for the binding of ethanol to graphene.[18] The adsorption energy of a single ethanol molecule on fluorographene (−8.7 kcal/mol) was lower than on graphene (−7.7 kcal/mol). On the other hand, the adsorption energies of ethanol clusters on fluorographene were higher than on graphene (−11.2 kcal/mol on fluorographene compared to −15.6 kcal/mol for $(EtOH)_4$ on graphene[18]). This different adsorption behavior of molecules and clusters is probably due to competition between H-bonding in the cyclic ethanol clusters (as occurs on the graphene surface) and possible H-bonding between the OH group of an isolated ethanol molecule and the F atoms of fluorographene: the calculated O−F distance for the O−H···F H-bond was 3.2 Å for a single ethanol molecule positioned on a fluorographene surface such that its −OH moiety was situated in the middle of an F-triangle (Figure 5).

The calculations indicate that acetonitrile also formed clusters on the fluorographene surface: the calculated adsorption energy for a single acetonitrile molecule (−7.8 kcal/mol) was substantially less negative than those for acetonitrile dimers (−10.6 kcal/mol per molecule) or trimers (−10.9 kcal/mol per molecule). The flat antiparallel adsorption geometries predicted for acetonitrile clusters on the fluorographene surface (see Figure 6 for an image of the trimer) were very similar to those identified for free clusters.[38] The C−H···N hydrogen bonding within the acetonitrile clusters appeared to be weak[38] given the calculated d(C−N) distance of 3.4 Å, whereas the corresponding d(C−F) distances for the putative C−H···F bonds to the fluorinated surface ranged between 3.2 and 3.5 Å (Figure 6).

The clustering of acetone on fluorographene appeared to be less favorable than ethanol and acetonitrile because the adsorption energies of the acetone dimer (−10.9 kcal/mol) and trimer (−11.5 kcal/mol) were comparable to that for a single acetone molecule (−10.7 kcal/mol). The planar acetone clusters that were predicted to form on the fluorographene surface (Figure 6) do not adopt the typical cyclical structures of free acetone clusters.[39] However, the weak intracluster C−H···O═C hydrogen bonding (Figure 6, d(O−C) = 3.3 Å) observed on the fluorographene has also been observed in free acetone clusters.[39,40]

DOI: 10.1021/acs.jctc.6b01130
J. Chem. Theory Comput. 2017, 13, 1328−1340

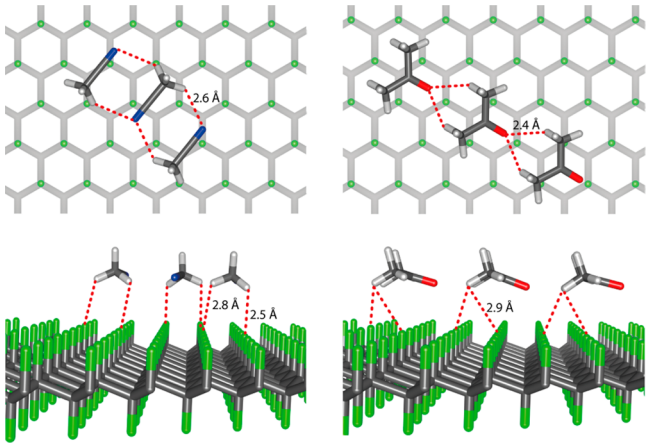

Figure 6. Top (top) and side (bottom) views of the adsorption geometries of acetonitrile (left) and acetone (right) trimers on fluorographene. Selected weak bonds between molecules in clusters (top) and between molecules and surfaces (bottom) are highlighted by red dotted lines. Structures were obtained by optimization with the optB86b-vdW density functional.

The difference in behavior of the ethanol, acetonitrile, and acetone molecules and other two adsorbates (as indicated by experiment) motivated us to perform additional calculations with ethyl acetate. We performed periodic calculations and evaluated the overall energy balance for the creation and adsorption of selected ethanol and ethyl acetate clusters. The thermodynamic cycle shown in the Scheme 1 explained the different behavior of ethanol and ethyl acetate on the surface, because the energy of clustering ΔE of ethanol molecules over the surface is negative (−2.5 kcal/mol) favoring formation of clusters, while the energy of clustering of ethyl acetate over the surface is close to zero (−0.3 kcal/mol). Typical enthalpy correction $\Delta H - \Delta E$ for the process of clustering is of order of 1 kcal/mol per molecule (e.g., $\Delta H - \Delta E$ corrections for ethanol clusters up to pentamer ranged between 0.9−1.4 kcal/mol per molecule[18]); therefore, enthalpy of clustering of ethyl acetate dimer from monomers on the surface will be positive, i.e., disfavoring formation of surface clusters.

2.8. Comparison of Measured and Computed Adsorption Enthalpies. The clustering on the fluorographene surface complicates direct comparisons of the measured adsorption enthalpies for the five molecular probes (Table 1) to those obtained from the calculations (Table 5). In fact, direct comparisons are only really justifiable for dichloromethane and ethyl acetate. We therefore corrected the adsorption enthalpies calculated for acetate, acetonitrile, and ethanol to account for the effects of clustering, as discussed in the preceding section. We also corrected the calculated ΔH values for adsorption to fluorographene (Table 5) using the correction terms calculated for fluorographite surface adsorption (Table S2) to enable meaningful comparison of the experimental and calculated quantities. A comparison of the experimental and modified computational results is presented in Figure 7.

All of the DFT methods systematically underestimated the strength of molecule/cluster binding to the fluorographite surface, i.e., the calculated ΔH values were always higher than the experimental values. The best accuracy was achieved with the optB86-vdW functional because its ΔH values were closer to the experimental results than those obtained with any other method. For clarity, only results obtained with this functional are shown in Figure 7. The inclusion of corrections for clustering always shifted the calculated adsorption enthalpies toward the experimental values. For dichloromethane and ethyl acetate, DFT methods that include dispersion corrections based on nonlocal correlation functional (i.e., optB86b-vdW, vdW-DF, and vdW-DF2) gave adsorption enthalpies that were closer to experiment than those that use corrections based on atom-centered empirical functions (DFT-DX methods). This trend opposes that observed in the benchmark calculations on small fluorographene models. It has many possible causes, ranging from the precise implementations of the empirically corrected DFT methods to the correct inclusion of many-body effects,[35,41] and warrants further investigation.

Scheme 1. Thermodynamic Cycle for the Creation of an Adsorbed Ethanol Tetramer (Left) and Ethyl Acetate Dimer (Right) on a Fluorographene/Fluorographite Surface Evaluated Using a Periodic Model[a]

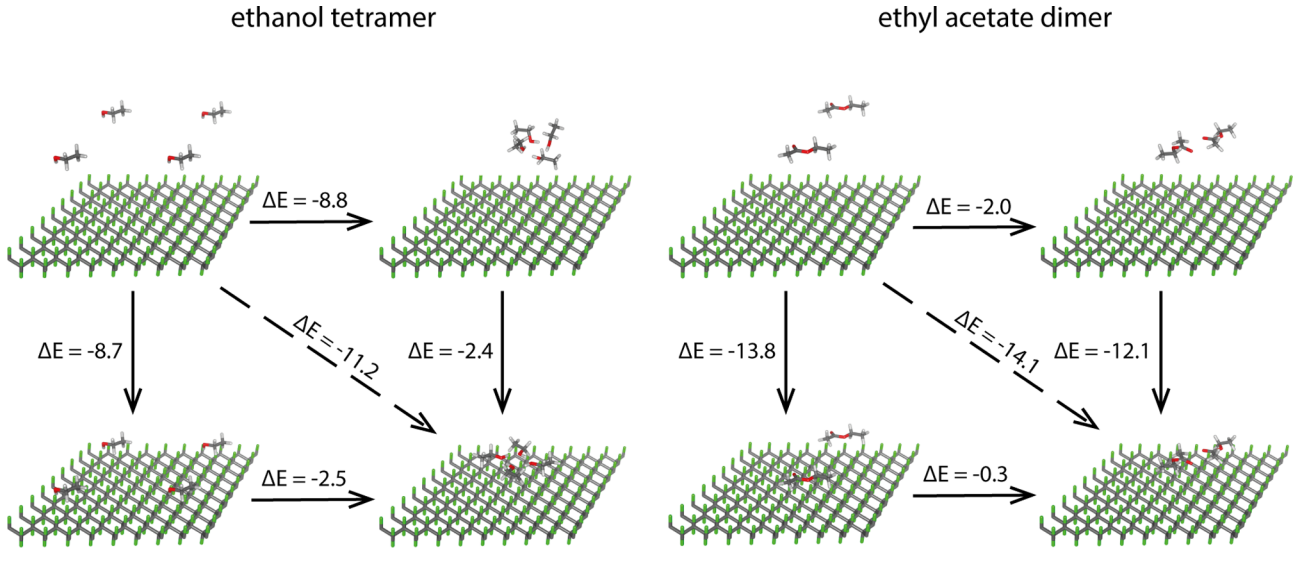

[a]All energies (in kcal/mol) are normalized to one ethanol (ethyl acetate) molecule.

DOI: 10.1021/acs.jctc.6b01130
J. Chem. Theory Comput. 2017, 13, 1328−1340

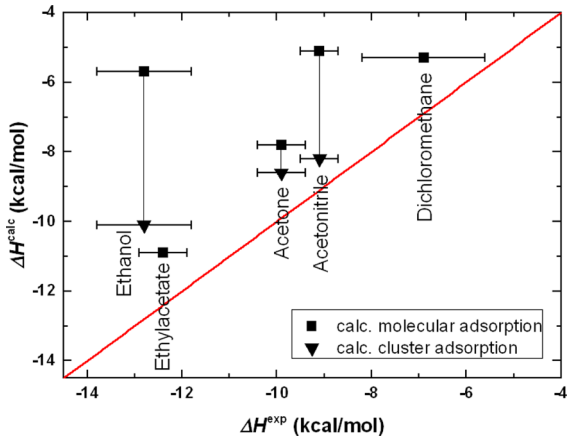

Figure 7. Experimental (Table 1, including error bar) and calculated adsorption enthalpies (ΔH). Calculated values corresponding to molecular adsorption (squares) were corrected for the effect of clustering (triangles). The red line represents perfect agreement between experiments and calculations. The calculated enthalpies are based on energies obtained with the optB86b-vdW density functional.

2.9. Isosteric Adsorption Entropies. The Langmuir adsorption model enabled enumeration of both the adsorption enthalpies and entropies. The entropies ranged from −19 cal/molK for dichloromethane to −36 cal/molK for ethanol. The overall trends in the adsorption entropies mirrored those for the adsorption enthalpies (Figure 1). It has previously been shown that the adsorption entropy of physisorbed molecules is surface-independent, being governed by the temperature and the gas phase entropy of the adsorbate.[42,43] This might explain the rather good agreement between the measured adsorption energies and those calculated for the finite fluorographene models (Table 1 and Table 4), although it is important to bear the effects of the experimentally observed clustering. The entropy loss upon adsorption corresponded to around 40% of the total gas phase entropy on average (Table S3 in the Supporting Information), which is consistent with previously published data.[42] A restriction of translational and rotational degrees of freedom of the adsorbed molecule was responsible for the entropy loss (Table S3). It should be noted that the discussed mirroring of entropies might indicate that stronger binding leads to larger entropy loss due to larger restriction of the probe conformational freedom on the surface.

3. CONCLUSIONS

We measured adsorption enthalpies of acetone, acetonitrile, dichloromethane, ethanol, and ethyl acetate on fluorographite by inverse gas chromatography at surface coverage levels ranging from 2 (0.2 for dichloromethane) to 20%. Plots of the resulting isosteric adsorption enthalpies revealed that acetone, acetonitrile, and ethanol cluster on the fluorographite/fluorographene surface. The other two molecules exhibited relatively coverage-independent adsorption enthalpies. The calculated saturated adsorption enthalpies on fluorographene ranged from −6.9 kcal/mol for dichloromethane to −12.8 kcal/mol for ethanol and were 1−2 kcal/mol lower than those previously determined for graphene. Computational investigations provided deeper insights into the strength and nature of adsorbate-fluorographene/fluorographite binding. Finite size models amenable to study using reference theoretical methods were a bit too small for reliable estimation of interaction energies but were useful in evaluating the accuracy of the adsorption energies calculated with various DFT methods because they permitted benchmarking against CCSD(T) and MP2.5 results. These benchmarking studies showed that dispersion corrected DFT functionals performed well and can be safely used for relative comparisons of adsorption energies. The finite size models also provided information on enthalpy corrections, which were rather modest, ranging from 1.3 to 1.5 kcal/mol. Despite the good performance of the dispersion-corrected functionals in the benchmarking study, nonlocal vdW DFT functionals (particularly optB86b-vdW) achieved the best agreement with experimental data when using a periodic model of fluorographene. Computational investigations using these functionals revealed that we did not detect binding to high-energy sites in the iGC experiments because binding to these structural features, which is typically very energetically favorable in layered materials, was either only slightly (by 10−20% for steps) more favorable or less favorable (in the case of edges) than binding to the surface. The adsorption enthalpies were largely controlled by the interaction energies, which were dominated by London dispersive forces. The clustering of ethanol, acetonitrile, and acetone on the fluorographene/fluorographite surface was explained by a delicate interplay between intracluster and cluster-surface bonding. Finally, we estimated adsorption entropies for the different adsorbates, which ranged from −19 cal/molK for dichloromethane to −36 cal/molK for ethanol and corresponded to a loss of ∼40% of the gas phase entropy upon adsorption. These results indicate that calculations on finite size models are adequate for estimating adsorption entropies on fluorographene surfaces.

4. EXPERIMENTAL AND COMPUTATIONAL METHODS

4.1. Chemicals and Experimental Setup. All measurements were conducted using an SMS iGC-SEA 2000 instrument (Surface Measurement Systems Ltd., UK) in a silanized column (3 mm diameter and 30 cm long) filled with a 23.9 mg sample of graphite fluoride (Sigma−Aldrich). Before each measurement, the sample was washed at 80 °C using He as the carrier gas at a flow rate of 10 sccm. A detailed characterization of the sample can be found in our previous article.[44] The used graphite fluoride crystals have a laminar morphology, and their surfaces are dominated by exposed fluorographene planes with a small proportion of edges and steps. Measurements were carried out with acetone (Merck, LiChrosolv, for HPLC, 99.8%), acetonitrile (Lach:ner, HPLC supergradient, min. 99.9%), dichloromethane (Merck, for LC LiChrosolv, ≥99.9%), ethanol (Merck, gradient grade for LC LiChrosolv, ≥99.9%), and ethyl acetate (Lach:ner, HPLC, min. 99,8%). Primary chromatograms were recorded at temperatures from 303 to 363 K using He as the carrier gas at the flow rate of 10 sccm. The column temperature was controlled by the instrument oven with declared stability of ±0.1 °C. Partial pressures of adsorbates were calculated from the primary chromatograms, i.e., peak maxima, using instrument calibration and Cirrus Plus Software advanced version 1.2.1.2 (Surface Measurement Systems Ltd., UK). The partial pressures of individual adsorbates were measured at the given targeted surface coverage ν_i as a function of temperature. The measurements were repeated for various target surface coverage ν_i, which ranged from 2% to 20% of monolayer. The saturated (40 °C) adsorbate vapors were injected into the column, and the injection time was set up to reach the targeted surface coverage. The required injection time was calculated from the targeted surface coverage, known surface area (236.9 m^2/g) of

DOI: 10.1021/acs.jctc.6b01130
J. Chem. Theory Comput. 2017, 13, 1328−1340

the material,[44] adsorbate vapor tension at 40 °C, and adsorbate cross sectional area using Cirrus Control Software advanced version 1.3.3 (Surface Measurement Systems Ltd., UK).

4.2. Data Analysis. The low surface coverage values considered in the experiments permitted application of the Langmuir adsorption model.[12,18,19] This assumption leads to the equation[18] $\frac{\nu_i}{1-\nu_i}\frac{p^{\phi}}{p} = e^{-(\Delta H_i - T\Delta S_i)/RT}$, which we used directly to fit the isosteric enthalpy of adsorption $\Delta H_i \pm \delta\Delta H_i$ and the entropy of adsorption $\Delta S_i \pm \delta\Delta S_i$ (Figure S3) for each considered target surface coverage ν_i. The partial pressure of the adsorbate, the standard pressure of 760 Torr, the universal gas constant, and the column temperature are denoted as p, p°, R, and T, respectively. The saturated adsorption enthalpy $\Delta H \pm \delta\Delta H$ was obtained as the mean value $\Delta H = \frac{1}{n}\sum_{i=1}^{n}\Delta H_i$ of n particular enthalpies obtained by fitting. The error in the saturated enthalpy, $\delta\Delta H$, was determined as the maximum individual $\delta\Delta H_i$ value. The same was done for the saturated entropy, $\Delta S \pm \delta\Delta S$.

4.3. Calculations. The adsorption energy, ΔE, was calculated as the difference between the energy of the most favorable configuration of the complex (comprising one molecule/cluster on fluorographene) and the sum of the energies of the optimized isolated species (fluorographene and the molecule in vacuum). In contrast, the interaction energy, ΔE_i, was calculated on the basis of each separated fragment in the geometry of the complex. The enthalpy of adsorption, ΔH, was calculated by adding the zero-point energy ($\Delta\Delta E_0$) and the thermal ($\Delta\Delta E_T$) and enthalpic ($\Delta\Delta E_H$) corrections to the adsorption energy, i.e., $\Delta H = \Delta E + \Delta\Delta E_0 + \Delta\Delta E_T + \Delta\Delta E_H$. The corrections $\Delta\Delta E_0$, $\Delta\Delta E_T$, and $\Delta\Delta E_H$ were evaluated for the molecule on a finite model of fluorographene, fully fluorinated tetracosahydrocoronene ($C_{24}F_{36}$), i.e., $\Delta H^{\text{fluorographene}} \approx \Delta E^{\text{fluorographene}} + (\Delta H^{C_{24}F_{36}} - \Delta E^{C_{24}F_{36}})$. For this purpose, geometry optimizations and frequency calculations were performed, and partition functions and thermochemical data (at 313.15 K and 101.325 kPa) were obtained. We used the B97D functional[45] and cc-pVTZ basis sets for all elements and the Gaussian09 package[46] for calculations on $C_{24}F_{36}$.

Reference wave function-based calculations of interaction energies ΔE_i were performed with a small finite model of fluorographene, perfluorohexamethylcyclohexane ($C_{12}F_{24}$). Accurate and computationally demanding CCSD(T)/complete basis set limit (CBS) interaction energies were determined using the formula[24]

$$\Delta E_i^{\text{CCSD(T)/CBS}} = \Delta E_i^{\text{MP2/CBS}} + (\Delta E_i^{\text{CCSD(T)}} - \Delta E_i^{\text{MP2}})_{\text{6-31G**(0.25,0.15)}}$$

Here, the CCSD(T) correction term was determined as the difference between the CCSD(T) and MP2 interaction energies with the 6-31G**(0.25,0.15) basis set. The basis set 6-31G**(0.25,0.15) is a modified version of the 6-31G** basis set in which the exponential parameters of the polarization functions were altered from their original values to 0.25 (C, N, F, O atoms) and 0.15 (H atom). The MP2/CBS interaction energies were determined by summing the Hartree−Fock and MP2 correlation energy components, $\Delta E_i = \Delta E_i^{HF} + \Delta E_i^{corr}$, both of which were extrapolated from the aug-cc-pVDZ (aDZ) and aug-cc-pVTZ (aTZ) basis sets.[24,47,48]

Alternative calculations were performed using the MP2-F12 method and the cc-pVDZ-F12 basis set to evaluate interaction energies. In these calculations, the core electrons were frozen, and interaction energies were corrected for the basis set superposition error (BSSE).[49]

The MP2.5/CBS interaction energies obtained for both the previously mentioned finite models were calculated using the following extrapolation equation[24]

$$\Delta E_i^{\text{MP2.5/CBS}} = \Delta E_i^{\text{MP2/CBS}} + 0.5(\Delta E_i^{\text{MP3}} - \Delta E_i^{\text{MP2}})_{\text{6-31G**(0.25,0.15)}}$$

The MP2.5 correction term was computed as a difference between the MP3 and MP2 interaction energies with the 6-31G**(0.25,0.15) basis set. As an alternative to the CBS limit, explicitly correlated MP2-F12 was used without any extrapolation.[24] All reference calculations were performed in TurboMole 6.6[50] under the Cuby framework[51] with the exception of the MP2.5 correction terms, which were calculated in Molcas 8.0[52]

SAPT decomposition allows the interaction energy to be partitioned into physically meaningful components. For this purpose, we used DFT-SAPT[28] as implemented by Hesselmann et al.[53] in the Molpro program package,[54] and we collected SAPT components into four terms corresponding to electrostatics, exchange repulsion, induction, and dispersion:[28]

$$\Delta E_i^{\text{SAPT}} = \Delta E_i^{\text{elst}} + \Delta E_i^{\text{exch-rep}} + \Delta E_i^{\text{ind}} + \Delta E_i^{\text{disp}}$$

We used the LPBE0AC exchange-correlation potential for monomer calculations[53] and the cc-pVTZ basis set.

DFT calculations on periodic fluorographene and its finite models were performed using the projector-augmented wave (PAW) method in the Vienna Ab initio Simulation Package (VASP, version 5.3.5).[55,56] Empirically corrected density functionals (PBE-D2,[45] PBE-D3,[57] PBE-TS,[58] PBE-TS-SCS[59]) and nonlocal correlation functionals (vdW-DF,[60] vdW-DF2,[61] optB86b-vdW[62]) that approximately account for nonlocal dispersion interactions were employed. The fluorographene sheet was modeled using a 5 × 5 supercell ($C_{50}F_{50}$···molecule) or 7 × 7 supercell ($C_{98}F_{98}$···cluster) with a chair structure, which has been shown to be the most stable fluorographene conformer.[63] Input geometrical parameters for fluorographene were obtained by PBE optimization from our previous works[37,64] and were as follows: lattice constant of a = 2.61 Å, C−C bond length of 1.58 Å, C−F bond length of 1.38 Å, and C−C−C bond angle of 110.9 deg. Multilayer fluorographene structures were modeled by fluorographene sheets with AA stacking;[44,65] an interlayer lattice constant of c = 6 Å was used as an input for optimization. For instance, the bilayer step of fluorographene consists of two sheets in a 5 × 10 supercell with the second sheet reduced to a 5 × 5 supercell and terminated by 5 + 5 fluorine atoms (150 carbon and 160 fluorine atoms in total). As periodic boundary conditions were applied in all three dimensions, a periodicity of at least 20 Å in the out-of-plane direction was imposed to minimize (spurious) interactions between adjacent layers. The energy cutoff for the plane-wave (PW) expansion was set to 400 eV, a convergence criterion of 10^{-6} eV was used in the SCF cycle, and Γ-point calculations were performed. The positions of the atoms were relaxed using the conjugate gradient method until the forces on each atom were below 1 meV/Å. For the final geometries of the 5 × 5 supercells, we recalculated all total energies with the 3 × 3 k-point mesh and an energy cutoff of 500 eV (see Table S4 for the convergence test).

Finally, the interaction energies for the $C_{24}F_{36}$ complexes were also calculated by DFT using Gaussian orbitals. Several functionals (B97D,[45] B3LYP,[66,67] and PBE[68]) and TZVPP[69]

DOI: 10.1021/acs.jctc.6b01130
J. Chem. Theory Comput. 2017, 13, 1328−1340

basis sets were used in conjunction with the empirical D3 dispersion correction;[57] the hybrid meta M06-2X[70] functional was used with the cc-pVTZ basis set.

■ ASSOCIATED CONTENT

Supporting Information

The Supporting Information is available free of charge on the ACS Publications website at DOI: 10.1021/acs.jctc.6b01130.

DFT-SAPT components of the interaction energies; calculated adsorption energies for single and double layered fluorographene; components of the adsorption entropy; convergence of the adsorption energy for periodic calculations; a plot of the adsorption enthalpy and entropy for dichloromethane at coverage levels ranging from 0.025 to 2%; data on the dependence of the interaction energy for ethanol on the surface model and method used; interaction energy curves for molecules and fluorographene; details on the enthalpy fitting procedure; and Cartesian coordinates for molecules adsorbed on finite models of fluorographene (PDF)

■ AUTHOR INFORMATION

Corresponding Author

*Phone: +420 585 634 756. E-mail: michal.otyepka@upol.cz.

ORCID

František Karlický: 0000-0002-2623-3991
Petr Jurečka: 0000-0002-3741-3672
Pavel Hobza: 0000-0001-5292-6719
Michal Otyepka: 0000-0002-1066-5677

Notes

The authors declare no competing financial interest.

■ ACKNOWLEDGMENTS

The authors gratefully acknowledge support from the Ministry of Education, Youth and Sports of the Czech Republic (LO1305 and CZ.1.05/2.1.00/19.0377) and the Czech Science Foundation (P208/12/G016). Funding from the European Union's Horizon 2020 research and innovation programme to M.O. under grant agreement No. 683024 (ERC-CoG) is gratefully acknowledged. M.O. thanks Neuron fund for support of science. M. Pitonak was supported by the Slovak Grant Agency VEGA under the contract No. 1/0092/14. M. Pykal was supported by the student project of Palacký University (IGA_PrF_2016_028). This work was part of the Research Project RVO: 61388963 of the Institute of Organic Chemistry and Biochemistry, Academy of Sciences of the Czech Republic.

■ REFERENCES

(1) Schwierz, F. Graphene transistors. *Nat. Nanotechnol.* **2010**, *5*, 487−496.
(2) Naik, A. K.; Hanay, M. S.; Hiebert, W. K.; Feng, X. L.; Roukes, M. L. Towards single-molecule nanomechanical mass spectrometry. *Nat. Nanotechnol.* **2009**, *4*, 445−450.
(3) Schedin, F.; Geim, A. K.; Morozov, S. V.; Hill, E. W.; Blake, P.; Katsnelson, M. I.; Novoselov, K. S. Detection of individual gas molecules adsorbed on graphene. *Nat. Mater.* **2007**, *6*, 652−655.
(4) Ambrosi, A.; Chua, C. K.; Bonanni, A.; Pumera, M. Electrochemistry of Graphene and Related Materials. *Chem. Rev.* **2014**, *114*, 7150−7188.
(5) Kulkarni, G. S.; Reddy, K.; Zang, W. Z.; Lee, K.; Fan, X. D.; Zhong, Z. H. Electrical Probing and Tuning of Molecular Physisorption on Graphene. *Nano Lett.* **2016**, *16*, 695−700.
(6) Nair, R. R.; Ren, W. C.; Jalil, R.; Riaz, I.; Kravets, V. G.; Britnell, L.; Blake, P.; Schedin, F.; Mayorov, A. S.; Yuan, S. J.; Katsnelson, M. I.; Cheng, H. M.; Strupinski, W.; Bulusheva, L. G.; Okotrub, A. V.; Grigorieva, I. V.; Grigorenko, A. N.; Novoselov, K. S.; Geim, A. K. Fluorographene: A Two-Dimensional Counterpart of Teflon. *Small* **2010**, *6*, 2877−2884.
(7) Robinson, J. T.; Burgess, J. S.; Junkermeier, C. E.; Badescu, S. C.; Reinecke, T. L.; Perkins, F. K.; Zalalutdniov, M. K.; Baldwin, J. W.; Culbertson, J. C.; Sheehan, P. E.; Snow, E. S. Properties of Fluorinated Graphene Films. *Nano Lett.* **2010**, *10*, 3001−3005.
(8) Zbořil, R.; Karlický, F.; Bourlinos, A. B.; Steriotis, T. A.; Stubos, A. K.; Georgakilas, V.; Šafářová, K.; Jančík, D.; Trapalis, C.; Otyepka, M. Graphene Fluoride: A Stable Stoichiometric Graphene Derivative and its Chemical Conversion to Graphene. *Small* **2010**, *6*, 2885−2891.
(9) Urbanová, V.; Karlický, F.; Matěj, A.; Šembera, F.; Janoušek, J.; Perman, J. A.; Ranc, V.; Čépe, K.; Michl, J.; Otyepka, M.; Zbořil, R. Fluorinated graphenes as advanced biosensors - Effect of fluorine coverage on electron transfer properties and adsorption of biomolecules. *Nanoscale* **2016**, *8*, 12134−12142.
(10) Cheng, H. S.; Sha, X. W.; Chen, L.; Cooper, A. C.; Foo, M. L.; Lau, G. C.; Bailey, W. H.; Pez, G. P. An Enhanced Hydrogen Adsorption Enthalpy for Fluoride Intercalated Graphite Compounds. *J. Am. Chem. Soc.* **2009**, *131*, 17732−17733.
(11) Seydou, M.; Lassoued, K.; Tielens, F.; Maurel, F.; Raouafi, F.; Diawara, B. A DFT-D study of hydrogen adsorption on functionalized graphene. *RSC Adv.* **2015**, *5*, 14400−14406.
(12) Lazar, P.; Karlický, F.; Jurečka, P.; Kocman, M.; Otyepková, E.; Šafářová, K.; Otyepka, M. Adsorption of Small Organic Molecules on Graphene. *J. Am. Chem. Soc.* **2013**, *135*, 6372−6377.
(13) Schrier, J. Fluorinated and Nanoporous Graphene Materials As Sorbents for Gas Separations. *ACS Appl. Mater. Interfaces* **2011**, *3*, 4451−4458.
(14) Reatto, L.; Galli, D. E.; Nava, M.; Cole, M. W. Novel behavior of monolayer quantum gases on graphene, graphane and fluorographene. *J. Phys.: Condens. Matter* **2013**, *25*, 443001.
(15) Campbell, C. T.; Sellers, J. R. V. Enthalpies and Entropies of Adsorption on Well-Defined Oxide Surfaces: Experimental Measurements. *Chem. Rev.* **2013**, *113*, 4106−4135.
(16) Ho, R.; Heng, J. Y. Y. A Review of Inverse Gas Chromatography and its Development as a Tool to Characterize Anisotropic Surface Properties of Pharmaceutical Solids. *KONA* **2013**, *30*, 164−180.
(17) Mohammadi-Jam, S.; Waters, K. E. Inverse gas chromatography applications: A review. *Adv. Colloid Interface Sci.* **2014**, *212*, 21−44.
(18) Karlický, F.; Otyepková, E.; Banáš, P.; Lazar, P.; Kocman, M.; Otyepka, M. Interplay between Ethanol Adsorption to High-Energy Sites and Clustering on Graphene and Graphite Alters the Measured Isosteric Adsorption Enthalpies. *J. Phys. Chem. C* **2015**, *119*, 20535−20543.
(19) Lazar, P.; Otyepková, E.; Banáš, P.; Fargašová, A.; Šafářová, K.; Lapčík, L.; Pechoušek, J.; Zbořil, R.; Otyepka, M. The Nature of High Surface Energy Sites in Graphene and Graphite. *Carbon* **2014**, *73*, 448−453.
(20) Otyepková, E.; Lazar, P.; Čépe, K.; Tomanec, O.; Otyepka, M. Organic adsorbates have higher affinities to fluorographene than to graphene. *Appl. Mater. Today* **2016**, *5*, 142−149.
(21) Karlický, F.; Lazar, P.; Dubecký, M.; Otyepka, M. Random Phase Approximation in Surface Chemistry: Water Splitting on Iron. *J. Chem. Theory Comput.* **2013**, *9*, 3670−3676.
(22) Pykal, M.; Jurečka, P.; Karlický, F.; Otyepka, M. Modelling of graphene functionalization. *Phys. Chem. Chem. Phys.* **2016**, *18*, 6351−6372.
(23) Karlický, F.; Lepetit, B.; Lemoine, D. Quantum modelling of hydrogen chemisorption on graphene and graphite. *J. Chem. Phys.* **2014**, *140*, 124702.
(24) Řezáč, J.; Hobza, P. Benchmark Calculations of Interaction Energies in Noncovalent Complexes and Their Applications. *Chem. Rev.* **2016**, *116*, 5038−71.

(25) Grimme, S.; Hansen, A.; Brandenburg, J. G.; Bannwarth, C. Dispersion-Corrected Mean-Field Electronic Structure Methods. *Chem. Rev.* **2016**, *116*, 5105−5154.
(26) Dubecký, M.; Mitas, L.; Jurečka, P. Noncovalent Interactions by Quantum Monte Carlo. *Chem. Rev.* **2016**, *116*, 5188−5215.
(27) Dubecký, M. Quantum Monte Carlo for Noncovalent Interactions: A Tutorial Review. *Acta Phys. Slovaca* **2014**, *64*, 501−575.
(28) Szalewicz, K. Symmetry-adapted perturbation theory of intermolecular forces. *Wires Comput. Mol. Sci.* **2012**, *2*, 254−272.
(29) Sedlák, R.; Riley, K. E.; Řezáč, J.; Pitoňák, M.; Hobza, P. MP2.5 and MP2.X: Approaching CCSD(T) Quality Description of Noncovalent Interaction at the Cost of a Single CCSD Iteration. *ChemPhysChem* **2013**, *14*, 698−707.
(30) Grimme, S. Density functional theory with London dispersion corrections. *Wires Comput. Mol. Sci.* **2011**, *1*, 211−228.
(31) Řezáč, J.; Huang, Y. H.; Hobza, P.; Beran, G. J. O. Benchmark Calculations of Three-Body Intermolecular Interactions and the Performance of Low-Cost Electronic Structure Methods. *J. Chem. Theory Comput.* **2015**, *11*, 3065−3079.
(32) Pitoňák, M.; Neogrády, P.; Hobza, P. Three- and four-body nonadditivities in nucleic acid tetramers: a CCSD(T) study. *Phys. Chem. Chem. Phys.* **2010**, *12*, 1369−1378.
(33) Brandenburg, J. G.; Maas, T.; Grimme, S. Benchmarking DFT and semiempirical methods on structures and lattice energies for ten ice polymorphs. *J. Chem. Phys.* **2015**, *142*, 124104.
(34) Grimme, S. Supramolecular Binding Thermodynamics by Dispersion-Corrected Density Functional Theory. *Chem. - Eur. J.* **2012**, *18*, 9955−9964.
(35) Bučko, T.; Lebégue, S.; Gould, T.; Ángyán, J. G. Many-body dispersion corrections for periodic systems: an efficient reciprocal space implementation. *J. Phys.: Condens. Matter* **2016**, *28*, 045201.
(36) Sato, Y.; Itoh, K.; Hagiwara, R.; Fukunaga, T.; Ito, Y. On the so-called "semi-ionic" C-F bond character in fluorine-GIC. *Carbon* **2004**, *42*, 3243−3249.
(37) Karlický, F.; Otyepka, M. Band Gaps and Optical Spectra of Chlorographene, Fluorographene and Graphane from G(0)W(0), GW(0) and GW Calculations on Top of PBE and HSE06 Orbitals. *J. Chem. Theory Comput.* **2013**, *9*, 4155−4164.
(38) Mata, R. A.; Costa Cabral, B. J. Structural, energetic, and electronic properties of (CH3CN)(2−8) clusters by density functional theory. *J. Mol. Struct.: THEOCHEM* **2004**, *673*, 155−164.
(39) Guan, J. W.; Hu, Y. J.; Xie, M.; Bernstein, E. R. Weak carbonyl-methyl intermolecular interactions in acetone clusters explored by IR plus VUV spectroscopy. *Chem. Phys.* **2012**, *405*, 117−123.
(40) Tamenori, Y.; Takahashi, O.; Yamashita, K.; Yamaguchi, T.; Okada, K.; Tabayashi, K.; Gejo, T.; Honma, K. Hydrogen bonding in acetone clusters probed by near-edge x-ray absorption fine structure spectroscopy in the carbon and oxygen K-edge regions. *J. Chem. Phys.* **2009**, *131*, 174311.
(41) DiStasio, R. A.; von Lilienfeld, O. A.; Tkatchenko, A. Collective many-body van der Waals interactions in molecular systems. *Proc. Natl. Acad. Sci. U. S. A.* **2012**, *109*, 14791−14795.
(42) Campbell, C. T.; Sellers, J. R. V. The Entropies of Adsorbed Molecules. *J. Am. Chem. Soc.* **2012**, *134*, 18109−18115.
(43) Savara, A.; Schmidt, C. M.; Geiger, F. M.; Weitz, E. Adsorption Entropies and Enthalpies and Their Implications for Adsorbate Dynamics. *J. Phys. Chem. C* **2009**, *113*, 2806−2815.
(44) Lazar, P.; Otyepková, E.; Karlický, F.; Čépe, K.; Otyepka, M. The surface and structural properties of graphite fluoride. *Carbon* **2015**, *94*, 804−809.
(45) Grimme, S. Semiempirical GGA-Type Density Functional Constructed with a Long-Range Dispersion Correction. *J. Comput. Chem.* **2006**, *27*, 1787−1799.
(46) Frisch, M. J.; Trucks, G. W.; Schlegel, H. B.; Scuseria, G. E.; Robb, M. A.; Cheeseman, J. R.; Scalmani, G.; Barone, V.; Mennucci, B.; Petersson, G. A.; Nakatsuji, H.; Caricato, M.; Li, X.; Hratchian, H. P.; Izmaylov, A. F.; Bloino, J.; Zheng, G.; Sonnenberg, J. L.; Hada, M.; Ehara, M.; Toyota, K.; Fukuda, R.; Hasegawa, J.; Ishida, M.; Nakajima, T.; Honda, Y.; Kitao, O.; Nakai, H.; Vreven, T.; Montgomery, J. A.; Peralta, J. E.; Ogliaro, F.; Bearpark, M.; Heyd, J. J.; Brothers, E.; Kudin, K. N.; Staroverov, V. N.; Kobayashi, R.; Normand, J.; Raghavachari, K.; Rendell, A.; Burant, J. C.; Iyengar, S. S.; Tomasi, J.; Cossi, M.; Rega, N.; Millam, J. M.; Klene, M.; Knox, J. E.; Cross, J. B.; Bakken, V.; Adamo, C.; Jaramillo, J.; Gomperts, R.; Stratmann, R. E.; Yazyev, O.; Austin, A. J.; Cammi, R.; Pomelli, C.; Ochterski, J. W.; Martin, R. L.; Morokuma, K.; Zakrzewski, V. G.; Voth, G. A.; Salvador, P.; Dannenberg, J. J.; Dapprich, S.; Daniels, A. D.; Farkas; Foresman, J. B.; Ortiz, J. V.; Cioslowski, J.; Fox, D. J. *Gaussian 09, Revision D.01*; Gaussian, Inc.: Wallingford, CT, 2009.
(47) Halkier, A.; Helgaker, T.; Jorgensen, P.; Klopper, W.; Koch, H.; Olsen, J.; Wilson, A. K. Basis-set convergence in correlated calculations on Ne, N-2, and H2O. *Chem. Phys. Lett.* **1998**, *286*, 243−252.
(48) Halkier, A.; Helgaker, T.; Jorgensen, P.; Klopper, W.; Olsen, J. Basis-set convergence of the energy in molecular Hartree-Fock calculations. *Chem. Phys. Lett.* **1999**, *302*, 437−446.
(49) Boys, S. F.; Bernardi, F. Calculation of Small Molecular Interactions By Differences of Separate Total Energies - Some Procedures with Reduced Errors. *Mol. Phys.* **1970**, *19*, 553.
(50) Furche, F.; Ahlrichs, R.; Hattig, C.; Klopper, W.; Sierka, M.; Weigend, F. Turbomole. *Wires Comput. Mol. Sci.* **2014**, *4*, 91−100.
(51) Řezáč, J. Cuby: An integrative framework for computational chemistry. *J. Comput. Chem.* **2016**, *37*, 1230−7.
(52) Aquilante, F.; Autschbach, J.; Carlson, R. K.; Chibotaru, L. F.; Delcey, M. G.; De Vico, L.; Fdez. Galvan, I.; Ferre, N.; Frutos, L. M.; Gagliardi, L.; Garavelli, M.; Giussani, A.; Hoyer, C. E.; Li Manni, G.; Lischka, H.; Ma, D. X.; Malmqvist, P. A.; Muller, T.; Nenov, A.; Olivucci, M.; Pedersen, T. B.; Peng, D. L.; Plasser, F.; Pritchard, B.; Reiher, M.; Rivalta, I.; Schapiro, I.; Segarra-Marti, J.; Stenrup, M.; Truhlar, D. G.; Ungur, L.; Valentini, A.; Vancoillie, S.; Veryazov, V.; Vysotskiy, V. P.; Weingart, O.; Zapata, F.; Lindh, R. Molcas 8: New capabilities for multiconfigurational quantum chemical calculations across the periodic table. *J. Comput. Chem.* **2016**, *37*, 506−541.
(53) Hesselmann, A.; Jansen, G.; Schutz, M. Density-functional theory-symmetry-adapted intermolecular perturbation theory with density fitting: A new efficient method to study intermolecular interaction energies. *J. Chem. Phys.* **2005**, *122*, 014103.
(54) Werner, H. J.; Knowles, P. J.; Knizia, G.; Manby, F. R.; Schutz, M. Molpro: a general-purpose quantum chemistry program package. *Wires Comput. Mol. Sci.* **2012**, *2*, 242−253.
(55) Blochl, P. E. Projector Augmented-Wave Method. *Phys. Rev. B: Condens. Matter Mater. Phys.* **1994**, *50*, 17953−17979.
(56) Kresse, G.; Joubert, D. From Ultrasoft Pseudopotentials to the Projector Augmented-Wave Method. *Phys. Rev. B: Condens. Matter Mater. Phys.* **1999**, *59*, 1758−1775.
(57) Grimme, S.; Antony, J.; Ehrlich, S.; Krieg, H. A consistent and accurate ab initio parametrization of density functional dispersion correction (DFT-D) for the 94 elements H-Pu. *J. Chem. Phys.* **2010**, *132*, 154104.
(58) Tkatchenko, A.; Scheffler, M. Accurate Molecular Van Der Waals Interactions from Ground-State Electron Density and Free-Atom Reference Data. *Phys. Rev. Lett.* **2009**, *102*, 073005.
(59) Tkatchenko, A.; DiStasio, R. A.; Car, R.; Scheffler, M. Accurate and Efficient Method for Many-Body van der Waals Interactions. *Phys. Rev. Lett.* **2012**, *108*, 236402.
(60) Dion, M.; Rydberg, H.; Schroder, E.; Langreth, D. C.; Lundqvist, B. I. Van der Waals density functional for general geometries. *Phys. Rev. Lett.* **2004**, *92*, 246401.
(61) Lee, K.; Murray, E. D.; Kong, L. Z.; Lundqvist, B. I.; Langreth, D. C. Higher-accuracy van der Waals density functional. *Phys. Rev. B: Condens. Matter Mater. Phys.* **2010**, *82*, 081101.
(62) Klimeš, J.; Bowler, D. R.; Michaelides, A. Van der Waals Density Functionals Applied to Solids. *Phys. Rev. B: Condens. Matter Mater. Phys.* **2011**, *83*, 195131.
(63) Leenaerts, O.; Peelaers, H.; Hernandez-Nieves, A. D.; Partoens, B.; Peeters, F. M. First-principles investigation of graphene fluoride and graphane. *Phys. Rev. B: Condens. Matter Mater. Phys.* **2010**, *82*, 195436.

DOI: 10.1021/acs.jctc.6b01130
J. Chem. Theory Comput. 2017, 13, 1328−1340

(64) Karlický, F.; Zbořil, R.; Otyepka, M. Band gaps and structural properties of graphene halides and their derivates: A hybrid functional study with localized orbital basis sets. *J. Chem. Phys.* **2012**, *137*, 034709.
(65) Karlický, F.; Otyepka, M. Band gaps and optical spectra from single- and double-layer fluorographene to graphite fluoride: many-body effects and excitonic states. *Ann. Phys.* **2014**, *526*, 408−414.
(66) Becke, A. D. Density-Functional Thermochemistry 0.3. The Role of Exact Exchange. *J. Chem. Phys.* **1993**, *98*, 5648−5652.
(67) Lee, C. T.; Yang, W. T.; Parr, R. G. Development of the Colle-Salvetti Correlation-Energy Formula into a Functional of the Electron-Density. *Phys. Rev. B: Condens. Matter Mater. Phys.* **1988**, *37*, 785−789.
(68) Perdew, J. P.; Burke, K.; Ernzerhof, M. Generalized gradient approximation made simple. *Phys. Rev. Lett.* **1996**, *77*, 3865−3868.
(69) Schafer, A.; Huber, C.; Ahlrichs, R. Fully Optimized Contracted Gaussian-Basis Sets of Triple Zeta Valence Quality for Atoms Li to Kr. *J. Chem. Phys.* **1994**, *100*, 5829−5835.
(70) Zhao, Y.; Truhlar, D. G. The M06 suite of density functionals for main group thermochemistry, thermochemical kinetics, noncovalent interactions, excited states, and transition elements: two new functionals and systematic testing of four M06-class functionals and 12 other functionals. *Theor. Chem. Acc.* **2008**, *120*, 215−241.
(71) Svoboda, V.; Majer, V. *Enthalpies of Vaporization of Organic Compounds: A Critical Review and Data Compilation*; Blackwell Scientific Publications: Oxford, 1985; Vol. 32.

DOI: 10.1021/acs.jctc.6b01130
J. Chem. Theory Comput. 2017, 13, 1328−1340